

Evolving Mobile Cloud Gaming with 5G Standalone Network Telemetry

HAORAN WAN, Department of Computer Science, Princeton University

KYLE JAMIESON, Department of Computer Science, Princeton University

Mobile cloud gaming places the simultaneous demands of high capacity and low latency on the wireless network, demands that Private and Metropolitan-Area Standalone 5G networks are poised to meet. However, lacking introspection into the 5G Radio Access Network (RAN), cloud gaming servers are ill-poised to cope with the vagaries of the wireless last hop to a mobile client, while 5G network operators run mostly closed networks, limiting their potential for co-design with the wider internet and user applications. This paper presents *NG-Scope5G*, a passive, incrementally-deployable, and independently-deployable Standalone 5G network telemetry system that streams fine-grained RAN capacity, latency, and retransmission information to application servers to enable better millisecond scale, application-level decisions on offered load and bit rate adaptation than end-to-end latency measurements or end-to-end packet losses currently permit. We design, implement, and evaluate *TGaming*, a telemetry-enhanced game streaming platform, demonstrating exact congestion-control that can better adapt game video bitrate while simultaneously controlling end-to-end latency, thus maximizing game quality of experience. Our experimental evaluation on a production 5G Standalone network demonstrates a 178–249% Quality of Experience improvement versus two state-of-the-art cloud gaming applications.

1 INTRODUCTION

Mobile cloud gaming is a growing business: Amazon (Luna), Microsoft (Xbox Game Pass), and Nvidia (GeForce Now) all now offer services that stream games from the cloud to any desktop, laptop, tablet, mobile phone, or TV device, and Apple opening up the App Store to game streaming services [52]. The promise of a high-quality gaming experience without the need for expensive, custom hardware reflects the current trajectory of industry investment and consumer interest, with a majority thinking game streaming services will eventually replace expensive home consoles [42].

The caveat to this pull from the market is the challenge of ensuring a reliable and high-throughput last wireless hop to the mobile gaming device. With the smartphone being the preferred game streaming device, and the cellular network (Mobile 4G/5G, or 5G *Fixed Wireless Access* [35]) the last hop of about half of all game-streaming sessions [42], it is no surprise that players who stop

Authors' addresses: Haoran Wan, Department of Computer Science, Princeton University, 35 Olden Street, Princeton, New Jersey, 08544, hw8161@princeton.edu; Kyle Jamieson, Department of Computer Science, Princeton University, 35 Olden Street, Princeton, New Jersey, 08544, kylej@princeton.edu.

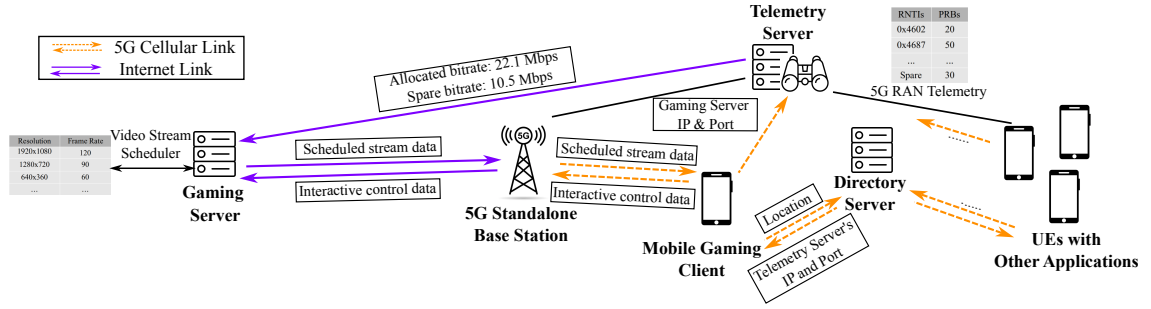


Fig. 1— TGaming: System Overview. TGaming’s **Cloud Gaming Server** receives exact capacity estimates of the 5G Standalone Radio Access Network from TGaming’s **5G Standalone Telemetry Server**, thus adjusting its video resolution and frame rate to accommodate the RAN’s capacity. While the scope of this paper is mobile cloud gaming, our telemetry tool is general, estimating spare capacity for any end-to-end transport protocol or application.

cloud gaming do so primarily because they perceive poor network quality [42]. High capacity, low latency, and high reliability of the last hop are all critical for a seamless user experience [18, 42].

Given the above status quo, the evolution of a reliable, low-latency, high-capacity 5G cellular network is key to ensuring success in the game streaming vertical, and many others [38]. Game streaming, and other new interactive applications, such as augmented reality and remote surgery, are intrinsically different from conventional video streaming, *e.g.*, because content server-to-eyeball latency must be low [11, 26], prohibiting buffering. 5G networks began operating in a *Non-Standalone* (NSA) mode with the 2018 3GPP Release 15 [2], which uses the 4G Evolved Packet Core, which limits performance. *5G Standalone* (SA) was introduced in the 2020 Release 16 [3], present in 2022 Release 17 [4], and is central to the ongoing phase of 5G deployment, *5G Advanced* (Release 18). It targets precisely the characteristics needed for game streaming: high throughput and low latency [40]. In parallel, many organizations are deploying *Private 5G* networks [39, 41]—*e.g.*, Linux Foundation Aether (formerly ONF Aether) [37]—to realize the performance benefits of Standalone mode at organizational scales. 5G Standalone is thus poised to become one of the main bearers for the last hop of mobile cloud gaming [42].

Yet even in this vibrant commercial landscape, the fundamental challenge that remains for cloud game platform designers is to cope with vagaries of the wireless Radio Access Network (RAN), where capacity changes drastically at millisecond-level scales due to fast fading associated with user mobility and cross-traffic from other users [57]. The game streaming server generates and sends video frames in real-time, in response to game play, which means that game play will stall if RAN capacity suddenly falls—the server must reduce its sending rate aggressively and instantly. Transport layer congestion control algorithms such as BBR [9], Copa [7], and CUBIC [17], video-on-demand applications [5, 15, 32], and live and interactive video streaming applications

[25, 51] generally rely on packet loss rates and one-way or round-trip latency measurements—a coarse-grained stream of information—to make their bit rate adjustment decisions. This can aggravate queuing in the RAN, which is also often the end-to-end bottleneck [29, 55].

Network telemetry of the RAN can address this challenge, passively listening to and parsing the operations of the RAN to provide granular physical-layer capacity measurements every millisecond, for every RAN user, without causing any interference to the network. Applications and transport layer protocols may then adjust the bit rate of their offered load and schedule their end-to-end flows more exactly, based on exact estimates of spare capacity, akin to XCP [23].

In this paper, we design and implement **TGaming**, a system that enhances mobile cloud gaming performance through telemetry for 5G Standalone (SA) operation. TGaming comprises two main components: NG-Scope5G, a *5G Standalone Telemetry Server* co-deployed with the RAN, and video frame scheduler and bit rate adaptation logic deployed at the *TGaming Gaming Server*. We design a rendezvous protocol that allows a mobile gaming client to discover a nearby TGaming telemetry server and prompt it to begin streaming telemetry data over the backhaul network (5G core and wide area internet), to the gaming server, eschewing the addition of any telemetry overhead to the wireless medium itself. Our telemetry server calculates each user’s fair share of any spare capacity, sending this information to the gaming server. After receiving NG-Scope5G telemetry, the NG-Scope5G-enabled gaming server adjusts its video frame scheduler, and encoding strategy to match the available downstream capacity.

Importantly, our design is *independently-deployable*: it requires no coordination nor cooperation with 1) 5G mobile network operators, 2) mobile device manufacturers (both with respect to hardware and software), nor 3) 5G cellular chipset manufacturers. Our experimental results show that TGaming can estimate network flow throughput with a 75th percentile error of less than 0.1% and detect individual data transmissions with an overall miss rate of 0.14% and 0.22% for downlink and uplink respectively. Our end-to-end evaluation of the TGaming cloud gaming platform demonstrates improved quality of experience (QoE) up to 249% compared with two state-of-the-art game streaming systems.

Our key contributions are summarized as follows:

- (1) We present the first (to our knowledge) Standalone-5G passive telemetry tool (*NG-Scope5G*) that can decode some RRC messages and all user control channel information for each user in a 5G SA RAN, at millisecond granularity.
- (2) We use NG-Scope5G’s telemetry to design an exact bit rate adaptation algorithm for cloud gaming. We design telemetry feedback within our target application’s RTSP session, decoupling it from other streams and thus providing a reusable infrastructure service for any future end-to-end application or transport layer protocol.

- (3) We evaluate TGaming on an open-source SA gNB (srsRAN gNB [48]/Open5GS core) and a commercial 5G SA gNB (Mosolabs *Canopy* small cell [34]/Aether Onramp [37] core) to demonstrate efficacy and broad applicability.

2 RELATED WORK

Mobile cloud gaming. Sunshine [31] is an open-source C++ cloud gaming server. Moonlight [16] is an open-source, multi-platform, NvStreams-based [36] cloud gaming client. Neither Sunshine nor Moonlight contain cellular specific performance optimizations. Nebula [6] is an end-to-end cloud gaming framework with a similar goal as the present work, which we compare against head-to-head in our performance evaluation. ZGaming [54] uses content-specific images to make frame predictions and reduce latency, (an approach orthogonal to TGaming), but needs to train a per-game basis.

Interactive video. Salsify [15] tightly integrates its video codec with a network transport protocol, while Sprout [53] uses packet arrival times at the receiver to adjust sending rates, but neither explores the use of RAN telemetry. Octopus [10] intentionally overestimates the server’s bit-rate, then drops packets at the 5G RAN, but requires coordination with the RAN designer and mobile operator, unlike TGaming.

On-Demand video streaming. MTP [59] develops a control theoretic adaptive bit rate (ABR) algorithm by solving the quality of experience maximization problem. Pensieve [32] generates ABR algorithms using reinforcement learning. Both rely on previous video chunks’ bit rates for their model inputs, which is slower and thus poorly-matched to game streaming. Oboe [5] tunes ABR parameters based on network conditions, while Bola [46] leverages Lyapunov optimization based on buffer levels at the client, but neither explores fast-changing cellular networks. Swift [12] employs layered neural video codecs and ML-based encoding to achieve fast reaction time. Big data ML network prediction algorithms have shown potential to improve video on demand [47, 58], but such studies aggregate broadband and wireless last hops, and so do not necessarily directly point to improvements for game streaming. However, we believe the combination of RAN telemetry data with these approaches has great potential. None of the foregoing supports real time video, making them hard to apply to the problem at hand.

Cellular telemetry. Most existing telemetry tools are specific to 4G LTE. On the handset, MobileInsight [30] and QXDM capture a variety of telemetry from different layers in the L1–L3 cellular stack, from a single UE’s perspective. In 4G, control information is in plaintext, so “sniffer” tools do not have to decode the RACH process (§3.2.2), but also cannot verify the correctness of the decoded information ([13, FALCON], [19, LTESniffer], and [56, NG-Scope]), whereas TGaming

can (§5.3). LTeye [27] does not handle MIMO, while OWL [8] lacks support for carrier aggregation. In contrast, TGaming targets 5G Standalone, with its more configurable control and data channels.

Industrial telemetry tools such as KeySight WaveJudge [24] and ThinkRF for 5G are closed source, generally require expensive and specialized hardware, and stop short of integration with end-to-end internet protocols and applications, which is the focus of the present work.

3 DESIGN

In this section, we elaborate on the system design of the TGaming cloud gaming platform, which comprises three main components: **1)** the TGaming Directory Server and **2)** the TGaming Video Stream Scheduler (both described in §3.1), and **3)** the NG-Scope5G 5G RAN Telemetry Server (described in §3.2).

Cloud gaming differs from conventional video streaming due to its highly interactive nature: the server computes and renders each users' viewport in real time, encodes the rendered views into compressed video frames, and sends the video frames to the mobile client. The TGaming scheduler (§3.1) works along with the video codec, which receives fine-grained data rate estimation from the NG-Scope5G telemetry server, adapting video resolution and frame rate to accommodate the network bandwidth. In this way, TGaming optimizes latency and frame rate, which are essential for improving QoE.

NG-Scope5G telemetry server (§3.2) is deployed physically near each cloud gaming user. It decodes 5G standalone RAN telemetry, calculates both allocated capacity and an estimate of fair-share spare capacity for each user in the cell. The telemetry server then sends these quantities back, end-to-end, to the cloud gaming server to convey these estimates in the coming milliseconds. Though there is a one-way delay lag in the reception, we later show that this granular time resolution fits particularly well with the real-time need of cloud gaming, as it allows TGaming to avoid building excess queues in the downlink direction.

3.1 Video Stream Scheduler

A mobile cloud gaming server and client set up multiple streams, including video, audio and player control data, using the real-time streaming protocol (RTSP) [43, 44], an application-level protocol for multiplexing and packetizing multimedia transport streams over a suitable transport layer protocol. Many cloud gaming platforms [21], as well as real-time video streaming and teleconferencing platforms use RTSP. According to our experiments (§5), video data comprises the greatest share of throughput among all cloud gaming streams, thus we focus there on video

¹In all figures, we denote TGaming's components with a black background.

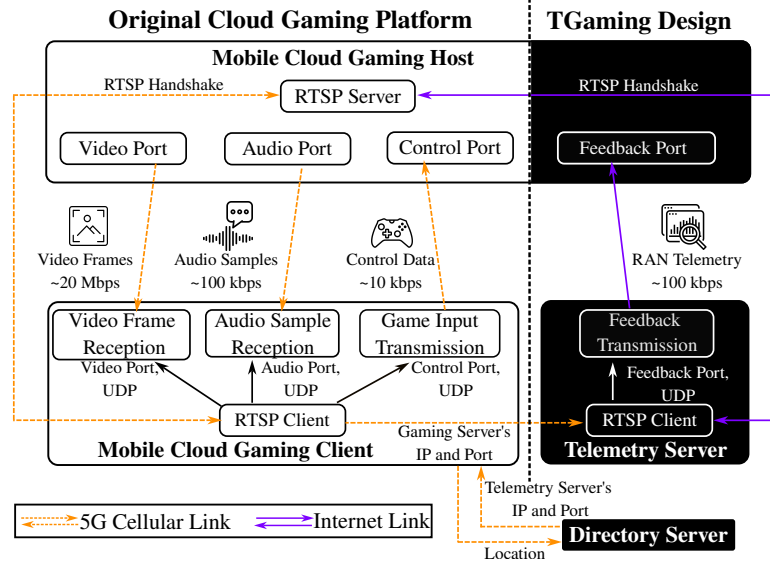


Fig. 2— Overview of TGaming's overall architecture.¹

stream optimization. Figure 2 shows the overall data flow of TGaming's data and control streams, with TGaming functionality highlighted.

3.1.1 Cloud Gaming Session Establishment. We design an RTSP-mediated feedback control stream establishment protocol for telemetry data that retains compatibility with Sunshine, as well as the aforementioned applications. In the startup stage, the client makes an RTSP handshake with the mobile cloud gaming server, during which both sides exchange a service description, such as each stream's port and network protocol, agree on parameters, and connect the client to these streams. This original handshake and the stream exchange process is represented by the arrow between RTSP server and client in the left-hand side of Fig. 2.²

Rendezvous. We envision the NG-Scope5G telemetry server (at bottom right in Fig. 2) as ubiquitously and incrementally-deployable infrastructure, located near clients (and 5G base stations), that measures the RAN's resource allocation constantly and passively. Before starting the gaming session, a client queries the TGaming Directory Server with a rough estimate of its location, obtained with standard mobile phone OS location services. The Directory Server replies with a list of IP addresses and ports of nearby NG-Scope5G telemetry servers.

Telemetry stream establishment. Also during game session establishment, the client software tells the telemetry server the IP address and port of the cloud gaming server, so the telemetry

²Further detail of these RTSP messages exchanged in the handshake is included in Appendix B.

server can set up a RAN Telemetry stream (see Fig. 2) with the gaming server in the same manner the mobile gaming client initiates other streams, *e.g.* video, audio, and control. This design incurs minimal burden on the mobile client and 5G RAN, because there are no hardware or cellular modem modifications required for the mobile client. It also has the advantage of adding no extra data burden to the RAN during the gameplay phase, as the RAN telemetry data itself traverses the RAN's (usually wired, or distinct and high-capacity point to point wireless) backhaul to the core network and then over wired links to the mobile cloud gaming server. With this RTSP initiated feedback design, the telemetry and stream scheduler is therefore fully decoupled from the original gaming or streaming operation, which provides more flexibility, and the client can decide whether to use it or not. During the gameplay phase, the cloud gaming server receives RAN telemetry from the telemetry server and uses it to optimize the downlink video stream.

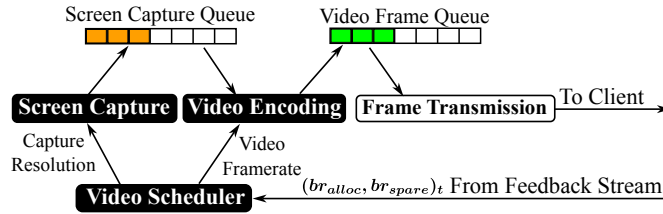


Fig. 3— Video capture and scheduling components at the TGaming game streaming server.

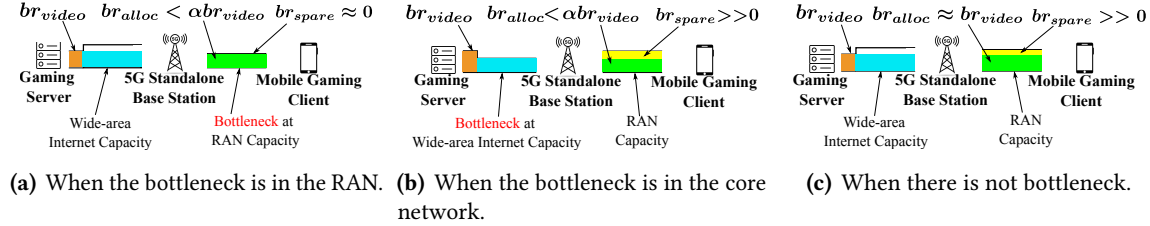


Fig. 4— The possible situations with bottleneck in different position of the network.

3.1.2 Gameplay. During the gameplay phase, the server's video processing consists of the three threads of execution shown in Fig. 3: screen capture, video encoding, and frame transmission. Unlike conventional video-on-demand transmission schemes that work on a per-*chunk* (a collection of video frames that lasts several seconds) basis [59], cloud gaming's video capture and transmission work on a per-frame basis. The client receives video frames from the server, decodes them also on a per-frame basis, and displays the frames on the screen. As long as the client can handle the video frames in real time, the client's buffer will not grow, and so the frame decoding capability of client sets the cap for the video stream scheduler's rate, which, in our case on a USD 200 phone, is 1080p video at 120 frames/s (fps).

Each element in the telemetry server–gaming server feedback stream consists of a tuple of 32-bit unsigned integers, indexed by transmission time interval t :

$$\left[(b_{alloc}, b_{spare})_t \right]. \quad (1)$$

The elements of this tuple represent the instantaneous (measured at time t) *bit-rate allocated to the user* and *spare bit-rate available in the RAN*, in units of bits per second. When the video scheduler needs to change one of the video stream’s parameters (resolution or frame rate), it raises a *reinit* event and adjusts the variable(s) corresponding to the changing parameter(s). The screen capture and video encoding threads check the status of this event after processing of each frame, if the *reinit* is raised, the two threads load the new values before they process the next frame. In this way, the scheduler is able to change the video stream’s resolution or frame rate within duration of one frame, *e.g.* 16.67 *ms* for 60 fps video.

During gameplay, the video scheduler actively compares the allocated and spare bit-rates from the feedback stream with the current bit-rate of the video stream to make real-time, millisecond-granularity scheduling decisions. To calculate the latter, we leverage Moonlight’s functionality (see §4 for further details) to map resolution and frame rate into a *current video bit rate* b_{video} (we denote this mapping f_{bw}):

$$b_{video} = f_{bw}(w, h, r), \quad (2)$$

where w and h are current video frames’ width and height in number of pixels, and r is current frame rate. Back-computing, given a desired video bit-rate b_{video} and a frame resolution (w, h) , we can calculate the frame rate r required to match this bit-rate: we denote this calculation f_{fps} . Similarly, fixing bit-rate and frame rate we calculate a corresponding frame resolution: we denote this calculation f_{res} .

Bit rate adaptation. The TGaming video scheduler inputs allocated and spare RAN bit rates and current video parameters, computes a target allocated bit rate, and from that, target video parameters for the next second of time.

The scheduler first estimates whether the end-to-end bottleneck link is located in the RAN, or elsewhere in the core or wide-area internet. If b_{video} exceeds $\alpha \cdot b_{alloc}$ (for a parameter $\alpha > 1$), then the cloud gaming server is sending at a faster rate than the RAN has allocated (as in Fig. 4(a)).³ If b_{spare} is also positive, then the end-to-end path’s bottleneck link is likely in the core network or wide-area internet because the excess packets are queuing at the bottleneck link and not saturating the RAN (as in Fig. 4(b))—in this case, we target an unchanged bit rate.

³We choose $\alpha \leftarrow 1.75$ here as a slightly loose bound to desensitize TGaming to imprecision in Moonlight’s bit rate estimation.

Otherwise, either the RAN is meeting the gaming server's offered bit rate (as in Fig. 4(c)), or it is saturated (possibly by other users as well), or both. We can therefore step up the offered bit rate to the extent there is spare capacity: we add b_{alloc} and a 75% of b_{spare} together to arrive at our new target bit rate. We can take all the b_{spare} in the RAN as in previous work [57], but the RAN may have different scheduling decisions so we take a conservative 75% of b_{spare} . Summarizing,

$$b'_{alloc} = \begin{cases} b_{alloc} & \text{if } b_{video} > \alpha \cdot b_{alloc}, b_{spare} > 0 \\ b_{alloc} + \frac{3}{4} b_{spare} & \text{otherwise.} \end{cases} \quad (3)$$

Algorithm 1 TGaming's video stream bit rate adaptation.

Input: $b_{r_{alloc}}, b_{r_{spare}}, w, h, r$
Output: w', h', r'
 $fps \leftarrow [90, 60, 45, 30, 15]$
 $b_{video} \leftarrow f_{bw}(w, h, r)$
if $b_{video} > \alpha b_{alloc}$ **then**
 $b'_{alloc} \leftarrow b_{alloc}$
else
 $b'_{alloc} \leftarrow b_{alloc} + 0.75 \cdot b_{spare}$
if $b'_{alloc} > b_{video}$ **then**
 if $w < w_{cap}$ and $h < h_{cap}$ **then**
 $w', h' \leftarrow f_{res}(b'_{alloc}, r);$
 $(w', h', r') \leftarrow (\max(w', w_{cap}), \max(h', h_{cap}), r)$
 else if $r < r_{cap}$ **then**
 $r' \leftarrow f_{fps}(b'_{alloc}, w, h)$
 $(w', h', r') \leftarrow (w, h, \max(r', r_{cap}))$
 else
 $r_{step} \leftarrow r$'s position in fps ;
 $w', h' \leftarrow f_{res}(b'_{alloc}, r);$
 while $w' < w_{bad}$ and $h' < h_{bad}$ and $r_{step} < 5$ **do**
 $r' \leftarrow fps[r_{step}]$
 $w', h' \leftarrow f_{res}(b'_{alloc}, r')$

The overall scheduling strategy is shown in Algorithm 1, where the $w_{cap}, h_{cap}, r_{cap}$ are the upper cap of video's w, h and r for the client's decoder.

Given our new target bit rate, we compute new target video parameters. If b'_{alloc} is bigger than the current video stream's bandwidth usage, b_{video} , we first fix the frame rate and increase the video's resolution until it reaches the resolution cap. If the video capture's resolution reaches its cap and there is still spare bandwidth, we then increase the frame rate for a more responsive experience. The reasoning behind this is that higher video resolution and fixed frame rate provide superior user mean opinion scores [22]. Conversely, when available bandwidth shrinks, we aggressively

Channel Name		Description and Relevance
PBCH	Physical Broadcast Channel	Signals a cell's existence to UEs and NG-Scope5G.
PDCCH	Physical Downlink Control Channel	Contains telemetry data locating network traffic and indicating its size.
PDSCH	Physical Downlink Shared Channel	Signals cell parameters to UEs and NG-Scope5G; delivers user data from the gNB to the UE.
RACH	Random Access Channel	Uplink channel used by the UE to rendezvous with the 5G service.

Table 1— 5G control and data channels, in order of their first appearance, and their relevance to NG-Scope5G.

decrease resolution and frame rate by first reducing the frame rate to a low preset value, and then gradually decreasing the resolution.

As available channel bandwidth continuously decreases, we first decrease the frame resolution. If the resolution drops under a threshold value, *e.g.* under 640×360 , denoted as w_{bad} and h_{bad} , we next decrease the frame rate. The frame rate setting steps are [90, 60, 45, 30, 15] fps. To achieve high QoE, we avoid changing the resolution at big steps, *e.g.* from 1080P to 720P. Instead, we adjust the resolution with smaller steps through f_{res} , such as decreasing 10% width and height pixels of 1920×1080 video frame into 1728×972 video frame. The mobile client's video decoder works well with such video resolution adjustments, and shrinking the resolution values gradually also helps to improve the user's experience because the resolution difference is not too obvious.

3.2 A Standalone 5G Telemetry Tool

The high-level goal of the NG-Scope5G telemetry tool is to decode and interpret *Downlink Control Information* (DCI), fine-grained telemetry information that the 5G TDD Radio Access Network (RAN) broadcasts onto the airwaves in the clear and which tells the mobile (referred to as the UE, for user equipment) where to receive its downlink data from or send its uplink data to in the physical data channels of the Standalone 5G TDD RAN, and thus how much data is actually present on those channels. We strive for an open design that operates independently of the 5G network operator and 5G mobile devices themselves, to decouple our design from any need to coordinate with these closed entities.

Preliminaries. The RAN divides time and frequency into *Physical Resource Blocks* (PRBs), equally-sized time-frequency blocks air that carry information to or from the base station, also known as a *cell*, or *gNodeB* (gNB). Time is divided into *slots*, or *Transmission Time Intervals* (TTIs) which are also the units of downlink-uplink transmission switching. Unlike the 4G LTE RAN, a sub-6 5G RAN can

have three different subcarrier spacings in the RACH process and later communication, including 15 kHz (same as 4G), 30, and 60 kHz, which result in TTIs of 1, 0.5, and 0.25 ms respectively.

Two key channels contain the relevant information: the *Physical Downlink Control Channel* (PDCCH), which in general carries control traffic from the gNB to the network, and the *Physical Downlink Shared Channel* (PDSCH), which delivers network traffic from the gNB to the UE. In general, DCI information in the PDCCH points to PRBs in the PDSCH containing both cell configuration information and network traffic. The *aggregation level* is the number of repetition for one DCI's transmission, e.g. downlink and uplink DCI uses different aggregation level in Figure 6, the gNB may use a higher aggregation level when channel conditions are poor, to ensure correct reception of DCI.

The *Cell Radio Network Temporary Identifier* (C-RNTI) is a unique identifier used in the RAN to identify a specific mobile device or UE.⁴ The cell assigns the UE a C-RNTI in an exchange in the *Random Access Channel* (RACH, see Table 1) between UE and gNB called the *RACH process*, which establishes a Radio Resource Control (RRC) session between UE and gNB [49]. RRC is a Layer-3 protocol whose major functions include connection establishment and release functions, and broadcast of system information.

An overview of NG-Scope5G's process is shown in Figure 5: the left side shows standard 5G RAN operation and the physical channels used for each message, while the right side shows our processing of telemetry, comprising the following high-level steps: 1) cell search and common (i.e., shared among all UEs) cell parameter acquisition (§3.2.1), 2) user identifier determination and UE-specific parameter acquisition (§3.2.2), 3) telemetry information extraction (§3.2.3), and 4) RAN capacity estimation (§3.2.4).

3.2.1 Cell Search and Cell Parameter Acquisition. The goal of this step is to discover the cell, and extract its channel configuration parameters, which describe the structure of the channel that the UE later uses to associate with the cell (§3.2.2). To make UEs aware of its existence, the base station periodically broadcasts basic information about itself in a *Master Information Block* (MIB), which includes a time index (the *system frame number*⁵) and configuration parameters of initial association. The MIB is the first message that the UE receives from a base station, and it is located in the *Physical Broadcast Channel* (PBCH, see Table 1). After decoding the MIB, the UE uses the information therein to locate PRBs that contain the *Control Resource Set* (CORESET) 0, a part of the larger PDCCH. CORESET 0 in particular carries a DCI that points to PRBs containing the next

⁴The *System Information Radio Network Temporary Identifier* (SI-RNTI) is the RNTI broadcast address, fixed as 0xFFFF by the 3GPP standard [4].

⁵One system frame is 10 ms, and the system frame number (0–1024), which the UE will also need to synchronize, indexes each system frame.

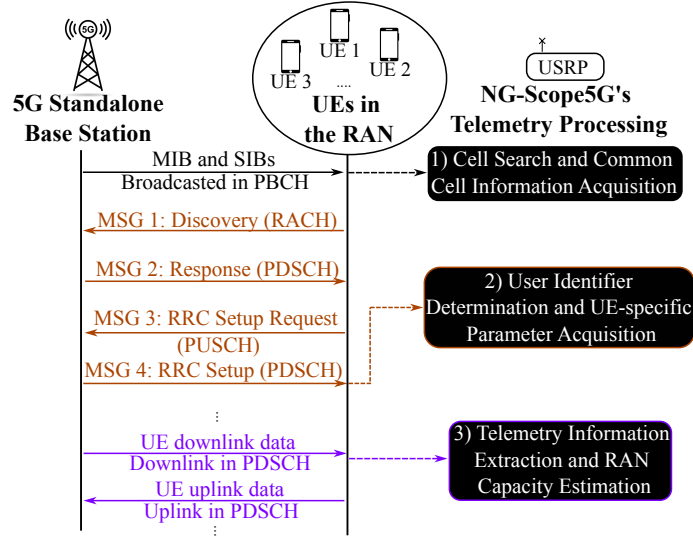


Fig. 5— NG-Scope5G telemetry design overview: NG-Scope5G passively listens to raw radio data and decodes radio resource control messages and DCIs from it. NG-Scope5G's processing components are denoted by a black background.

message we need to decode, the *System Information Block* (SIB) 1 in the PDSCH—this is illustrated in the lower-left corner of Fig. 6.

The SIB 1 (also broadcasted periodically in the PDSCH channel), carries common information about the cell, including physical channel configuration and all the information a UE may need for the RACH processing described next in §3.2.2, such as the subcarrier spacing for the cell in RACH process, the parameter and time-frequency position for MSG 1 in RACH, and aggregation level of the DCIs. We decode the DCI aggregation level from the SIB 1, obviating the need to blindly search levels as prior tools do [13, 56].

3.2.2 User Identifier and Parameter Determination. The goal of this step is to acquire the user's C-RNTI and the cell's parameters for the channel containing the final telemetry information we seek (the PDCCH, see Table 1). Since DCIs after the RACH process are all scrambled by a sequence derived from the C-RNTI, we decode the parts of the process required to extract the C-RNTI.

There are four messages exchanged between gNB and UE: MSG 1 (Preamble Transmission), MSG 2 (Random Access Response), MSG 3 (RRC Setup Request), and MSG 4 (RRC Setup), shown on the left side of Figure 5. SIB 1 tells the UE where and when to transmit MSG 1 to the cell, to begin the process.⁶ MSG 4 contains most of the UE-specific information required for mobile

⁶MSG 1 contains a synchronization sequence that makes the cell aware of the UE. MSG 2 contains timing adjustment, a temporary cell RNTI (TC-RNTI), and an initial uplink grant for the UE to transmit MSG 3. MSG 3 contains an RRC

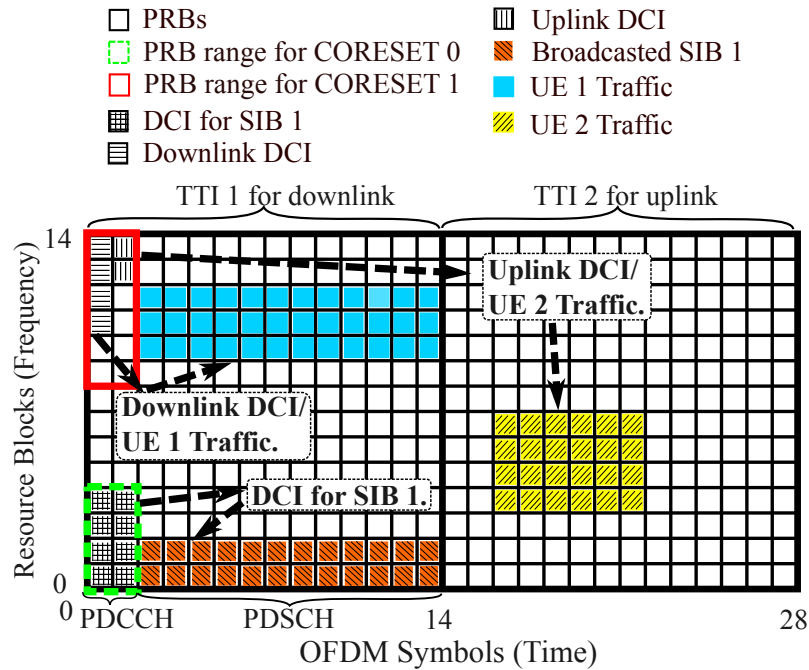


Fig. 6— An overview of DCI and data transmission in the 5G physical layer. There are multiple CORESETs, each of which occupies part of the bandwidth, and the DCIs point to the resource blocks that UE should receive from or send data to.

communication and for telemetry, such as position and search space of initial CORESET, and the aggregation level for DCI transmission. NG-Scope5G only decodes MSG 4, as the DCI for MSG 2 and 4 are not scrambled with the RNTI as is the case for other DCIs, but instead are in plain text, with a TC-RNTI-scrambled CRC of the DCI appended, the same as in 4G [1]. Knowing this, we can calculate the TC-RNTI by an exclusive-or of a CRC of the received DCI plain text computed by NG-Scope5G, and the appended TC-RNTI-scrambled CRC of the DCI, separately received by NG-Scope5G, as previous 4G sniffers [13, 56] do for each and every received DCI. When the TC-RNTI is promoted to the C-RNTI after MSG 4, we thus obtain the C-RNTI of the UE without decoding the preliminary messages and we can verify the correctness of decoded MSG 4 through CRC check. Then from MSG 4, we get the position of the CORESET, aggregation level of DCIs, correct format of DCI that the gNB and UE will use later data communication. A sample of MSG 4 can be found in Appendix C.2.

Setup request to the gNB. Then the UE and gNB will use the TC-RNTI for MSG 4, after which the UE is RRC connected to the gNB. The gNB promotes the TC-RNTI to a C-RNTI, and uses it for data communication later.

3.2.3 Telemetry Information Extraction. The goal of this step is to estimate the amount of data traffic in the data channel (PDSCH, see Table 1) for each UE in the RAN, and its associated physical layer parameters (bit rate and channel quality). Furthermore, the UE also gets the DCI format type and aggregation level from MSG 4 [4]⁷ Since we have decoded the required information, NG-Scope5G moves to the same *bandwidth part* (a fraction of the whole cell channel) as the UE for DCI reception at this stage. With all required information known (C-RNTI, aggregation level, DCI format), NG-Scope5G’s DCI reception process is the same as the standard 3GPP DCI decoding for each UE, where the detailed information can be found in [45, 49], which yields the 30–80 bits of DCI data.⁸

3.2.4 RAN Capacity Estimation. The goal of this step is to calculate the capacity (bit rate) allocated to each UE and the spare RAN capacity, through telemetry information.

With the DCI and all the RRC messages we decode from the previous stages, we calculate the *Transport Block Size* (TBS) for each DCI, whose value indicates how many bits are transmitted in this TTI, for the specific UE through this DCI. We calculate the TBS according to the 3GPP standard—it is a function of the error control coding rate, the modulation, the number and spacing of OFDM subcarriers, and framing overheads, whose details we leave to Appendix A. We record the TBS for every UE in every TTI, maintain a sliding window to calculate the bit rate for each UE, and we update the data rate in every TTI. Furthermore, in each TTI, we split unused PRBs evenly across UEs and recalculate these PRBs to yield a fair-share spare capacity attributable to each UE.

Due to wireless fading, the UE may fail to decode the downlink traffic, triggering re-transmission, in which case transport blocks contain old data that should not be considered in NG-Scope5G’s bit rate calculation. NG-Scope5G captures the re-transmission information in the physical and MAC layers through tracking Hybrid Automatic Repeat Request (HARQ) information in DCIs. The gNB allocates up to 16 HARQ processes for each UE, informing the UE of each process through `harq_id` in the DCI. If the UE correctly decodes the data in one TTI, it sends an ACK to the gNB, which then toggles the `new_data_indicator` (`ndi`) of the DCI with the same `harq_id` to indicate new data in the next TTI of the process. If the UE NACKs, the gNB uses the same `ndi` as the previous DCI with the same `harq_id` for the re-transmission. NG-Scope5G maintains a 16-element array for each UE to record the `ndi` from previous DCIs for each `harq_id` to detect re-transmissions, and sets the TBS for this TTI to zero if it is a re-transmission.

⁷For example, format 1-1 or 1-0 for downlink DCI—the sample configuration can be found at `searchSpacesToAddModList` in Appendix C.2.

⁸This includes deinterleaving and the modulation and coding scheme indicator, which are required for transport block size (TBS) calculation and our later capacity estimation. A sample of DCI with format 1-1 and its translated downlink grant for PDSCH can be found in Appendix C.3.

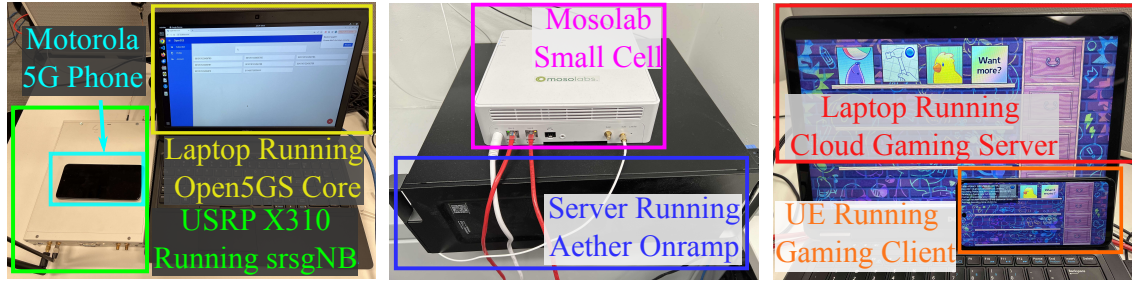


Fig. 7— Hardware used in the TGaming implementation.

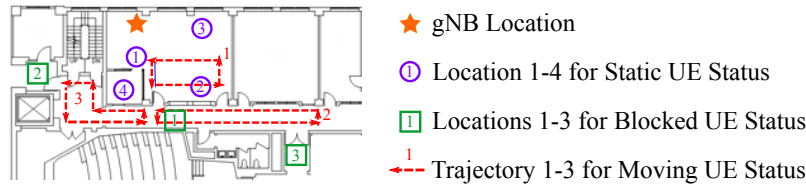


Fig. 8— Map of performance evaluation.

4 IMPLEMENTATION

We implement TGaming’s video stream scheduler on top of Sunshine and Moonlight with 621 lines of C++ code in the Sunshine server and 224 lines of Java code in the Moonlight [16] android client (excluding reused code). We extend the event-driven RTSP server to set up the feedback stream from NG-Scope5G’s telemetry server. The cloud gaming server receives two 32 bits unsigned integer feedback $(br_{alloc}, br_{spare})_t$ from telemetry server in a interval of 0.5 millisecond. It uses these values to make video scheduling decisions, changing resolution and frame rate in real time (§3.1). The client determines the availability of the telemetry server and sends the cloud gaming server’s address to the telemetry server.

We implement NG-Scope5G’s telemetry functionality in 3,839 lines of C++ code (excluding reused code) processing radio signals received by a USRP. We reuse the physical layer signal processing modules from an open-source 5G library srsRAN [48], *i.e.*, a wireless channel estimator, a demodulator, and a frame synchronizer. srsRAN only supports processing for a 10 MHz FDD base station with 15 kHz subcarrier spacing, thus we modify their low level processing code extensively, altering radio sample reception, Fourier transform scheduling and phase compensation, to support different subcarrier spacing, higher bandwidth and TDD base station processing, such as 30 kHz subcarrier spacing, 20 MHz bandwidth in the 5G TDD band. Then we implement the cell search, SIB 1 decoding, RACH decoding, DCI extraction and RAN throughput estimation on top of that. The telemetry server decodes the DCIs within every TTI and calculate the allocated bit rate and spare bit rate for each UE in the RAN.

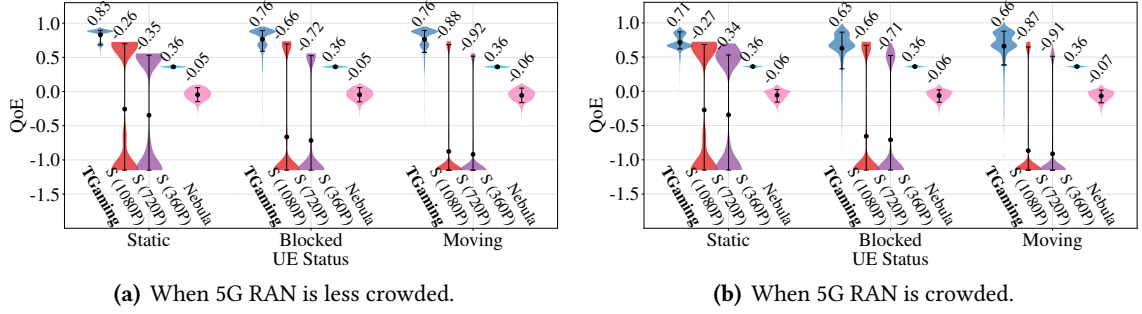


Fig. 9— QoE comparison: numbers above data points indicate mean QoE; whiskers denote 10th/90th percentiles (S: Sunshine).

5 EVALUATION

We proceed top-down, first introducing our overall methodology (§5.1), then evaluating end-to-end cloud gaming performance in terms of network utilization and QoE metrics (§5.2). Finally, we evaluate NG-Scope5G’s telemetry in terms of DCI decoding, PRB detection and flow throughput estimation accuracy (§5.3).

5.1 Methodology

We evaluate TCGaming in the following two real 5G Standalone networks, as shown in Fig. 7. In both networks, Motorola *Moto G* 5G phones serve as the clients.

[srsRAN/Open5GS]: In this open-source 5G Standalone network, we run [Open5GS](#) on a four-core CPU laptop with 8 GB of memory, and an srsRAN gNB [48] with a X310 USRP. The gNB runs on 5G New Radio band n41 in TDD mode, with downlink center frequency 2524.95 MHz, subcarrier spacing 30 kHz, and channel bandwidth 20 MHz.

[Mosolabs/Aether]: In this Private 5G Standalone network, we configure an Aether Onramp 5G software defined core network [37] on a 10-core CPU machine with 16 GB of memory, and a Sercomm Mosolabs small cell [34]. The gNB runs in the CBRS band (n48) in TDD mode, controlled by a spectrum access server (SAS) [14], on center frequency 3561.6 MHz, subcarrier spacing 30 kHz, and channel bandwidth 20 MHz.

5.2 Cloud Gaming Performance

In this part of the evaluation, we run the original and modified cloud gaming host on a 2-core CPU laptop with 8 GB of memory, and we run the original and modified moonlight client on one of the Motorola phones. We use our [Mosolabs/Aether] Private 5G Standalone network. All the foregoing machines run Ubuntu Linux 22.04.

5.2.1 Methodology. We compare the end-to-end performance of TGaming mobile cloud gaming head to head against Nebula [6] and Sunshine. Sunshine does not adjust bit rate, so we have enhanced it to run at 1080p, 720p, and 360p, at 60 fps. Nebula (described in §2) uses forward error correction to adjust its bitrate. We configure it and TGaming to use a maximum resolution of 1080p; both use their own ABR algorithms. Nebula is developed with Python and does not support Android devices. For a sound comparison, we run Nebula’s server code on the same laptop that we run Sunshine server on and connect the client to the 5G RAN by using USB tethering with the mobile phone.

In our experiments, we collect all the metrics from the mobile cloud gaming server and client in real time. For TGaming and Sunshine, we collect network packets and calculate downlink throughput by running tcpdump on the mobile client. We collect the video’s resolution inside the video scheduler and collect received frame rate, latency probing results, and packet loss rate on the client with moonlight built-in functions. For Nebula, we collect throughput by running tcpdump on the client laptop, and we collect resolution, frame rate, and latency probing results from its built-in logs. We calculate Nebula’s packet loss rate by comparing the actual number of frames received and the frame index.

We evaluate the performance of mobile cloud gaming using both network metrics and QoE metrics. Our network metrics contain goodput and one way delay. We select QoE metrics including video resolution, frame rate, network latency, and packet loss rate [28, 33] with overall QoE metric

$$\text{QoE} = \alpha R + \beta F - \gamma L - \delta P, \quad (4)$$

where α to δ are the weights for each parameters, R is the resolution, F is the frame rate, L is the network latency and P is the packet loss rate. We normalize all the parameters into range of $[0, 1]$ using min-max normalization, with the global maximal and minimal values in the evaluation. For resolution, we only use one axis of the screen (width/height) to perform normalization. We rank the importance of these parameters’ importance as: $P > F > L > R$, according to the importance analysis in [20, 22], and the weights are set as $\alpha = 0.5$, $\beta = 0.6$, $\gamma = 0.7$, and $\delta = 0.8$.

To evaluate under rigorous real-world scenarios, we measure the performance of TGaming (T), Sunshine (S), Nebula (N) under different settings: static, blocked and moving clients. Fig. 8 shows the UE’s locations and trajectories during this evaluation. We create two different RAN conditions—a less crowded RAN and a crowded RAN. For the less crowded RAN, we use other 3 UEs to watch Youtube live stream, where there are plenty of spare PRBs for the cloud gaming client. For the crowded RAN, we use the three other UEs to download big files from the Internet using UDP protocol to make the number of spare PRBs close to zero. For each UE and RAN status,

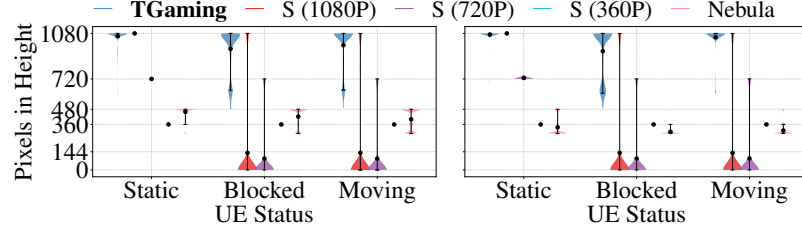


Fig. 10— Video playback resolution (S: Sunshine). Left: less crowded RAN; right: crowded RAN.¹⁰

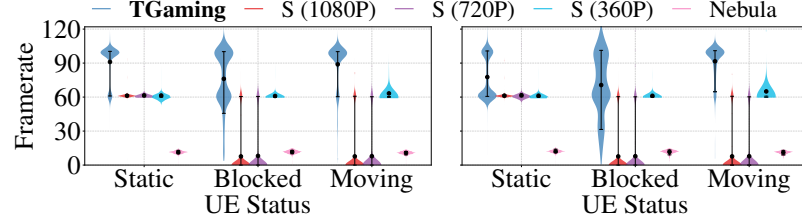


Fig. 11— Video frame rate in frames/second (S: Sunshine). Left: less crowded RAN; right: crowded RAN.¹⁰

we run each system for five minutes in static scenarios, and 2–3 minutes in the mobile scenarios⁹ and repeat this process five times.

5.2.2 QoE Evaluation. We evaluate all three systems under the experimental scenarios introduced above. Figs. 9 to 12, show the performance of all three systems in overall QoE and each individual QoE metric. Fig. 9 shows the overall QoE results, where TGaming has the best average QoE across all UE and RAN conditions. TGaming improves QoE by 178.3% and 249.2%, compared with Sunshine’s average QoE when the RAN is less crowded and more crowded, relatively. Sometimes (in blocked Locations 2 and 3 and moving trajectories 2 and 3) Sunshine stalls due to sending at too high a bit rate. Nebula has the lowest QoE result because it conservatively uses a low resolution and frame rate to maintain the seamless experience. When the UE is blocked or moving to the area where the signal is weak (blocked and moving UE scenarios), TGaming actively changes the resolution and frame rate, yielding a high variance in resolution and frame rate (in Figs. 10 and 11). Nebula uses a low resolution and low frame rate video in these conditions, which contributes to its low overall QoE results. As for packet loss rate, all three system have a low packet loss rate when the UE is static (Fig. 12), TGaming and Nebula has a slightly worse packet loss rate when the RAN is crowded. This evaluation shows that TGaming can improve the QoE when the RAN connection is ideal and help to overcome packet loss caused by a weak signal.

5.2.3 Network evaluation. We begin with an examination of the network usage properties of all three systems. We observe that Sunshine suffers outages in Loc. 2 and 3 in the blocked scenario,

⁹Some Nebula runs are shorter due to crashes, but all last at least two minutes, and our metrics do not penalize Nebula in these circumstances.

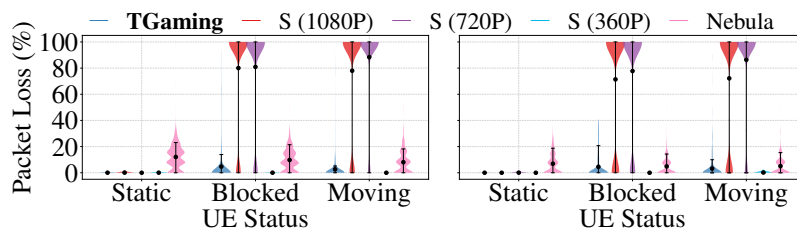


Fig. 12— Application-level packet loss rate (S: Sunshine). *Left: less crowded RAN; right: crowded RAN.*¹⁰

and Traj. 2 and 3 in the moving scenario, where its packet loss rate reaches 100%, while both TGaming and Nebula can work under these circumstances. Thus, we exhibit the results separately for these challenging environments. Fig. 13 shows the results: when the RAN is less crowded, TGaming achieves high throughput and low latency when channel quality is good (Fig. 13(a), Loc. 1 in Fig. 13(b) and Traj. 1 in Fig. 13(c)). Otherwise, (Loc. 2 and 3 in Fig. 13(b) and Traj. 2 and 3 in Fig. 13(c)), TGaming matches its bit rate to the RAN’s bit rate, which causes high throughput and latency variance. Sunshine maintains stable performance when the channel is good, but cannot adjust itself to accommodate a poor channel so loses its functionality. Nebula is conservative, keeping resolution and frame rate low to keep running in a poor network. When the RAN is crowded, TGaming increases its bit rate with the cost of higher variance in latency if the physical channel quality is good. In a weak channel, (Loc. 2 and 3 in Fig. 13(e) and Traj. 2 and 3 in Fig. 13(f)), both TGaming and Nebula provide a seamless experience, but Nebula makes a conservative bandwidth choices while TGaming better utilizes spare RAN capacity while maintaining low latency.

5.3 RAN Telemetry

We evaluate NG-Scope5G telemetry time series data, DCI miss rates, PRB decoding accuracy, RAN allocated throughput estimation accuracy, and wall clock processing time.

5.3.1 Time series. We demonstrate NG-Scope5G telemetry resolution through a time series shown in Fig. 14. During this demonstration, we connect 2 UEs to the [Mosolabs/Aether] network, then use both NG-Scope5G and tcpdump [50] on each phone to calculate each UE’s downlink network bandwidth. UE 1 plays a mobile cloud game through the moonlight mobile client and UE 2 is watching a live stream on Twitch. As we can see from Fig. 14(a), the capacity estimation for each UE is highly accurate in time (the curve tracks just under ground truth). Turning to Fig. 14(b) we see NG-Scope5G calculates the spare bit rate for each UE through the fair share of spare PRBs. Even though the number of fair share PRBs are the same for each UE, the calculated spare bit rates are different. This is because two UEs have different MCS indices and coding rates in the same TTI.

¹⁰In Figs. 10 to 12, the data series order matches the legend order.

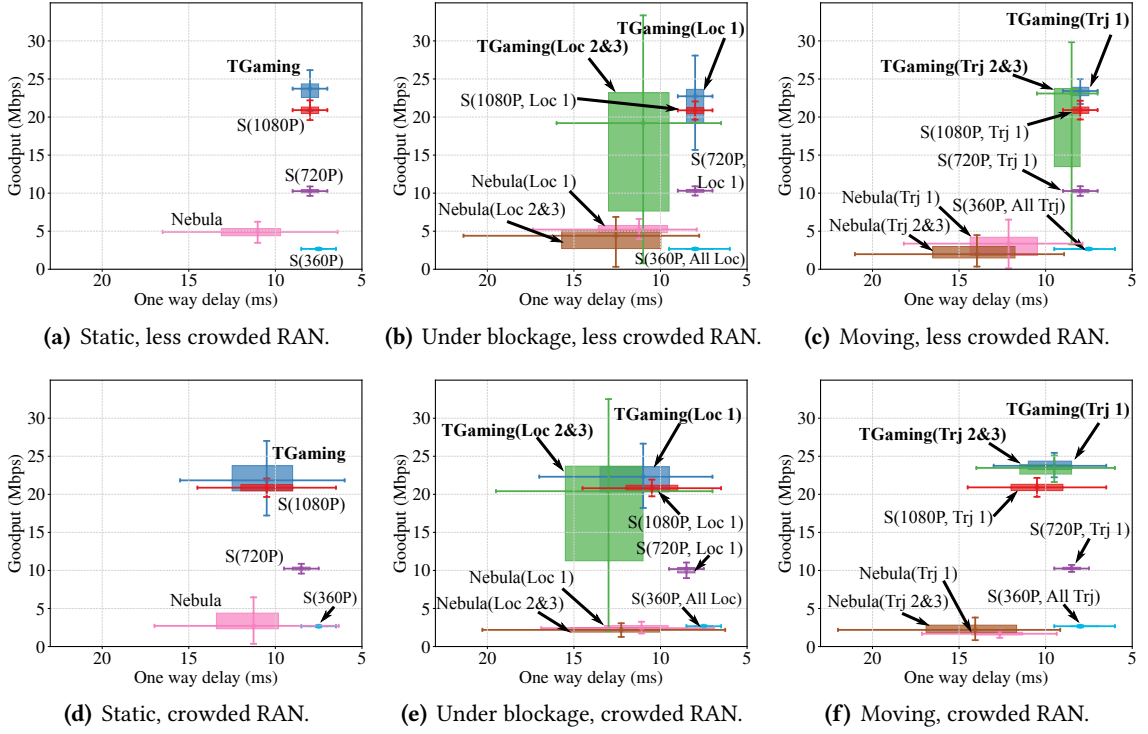


Fig. 13— Network usage comparison: TGaming, Sunshine (S), and Nebula. Boxes: middle quartiles; whiskers: extreme deciles.

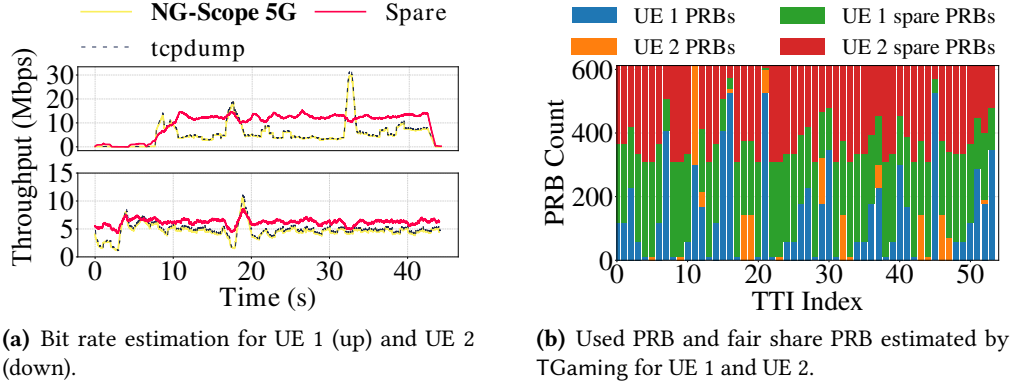


Fig. 14— NG-Scope5G telemetry example trace: We calculate the bit rate over time. Then we split the free PRBs equally among UEs and use the same parameters in used PRBs to calculate the bit rate provide by the free PRBs.

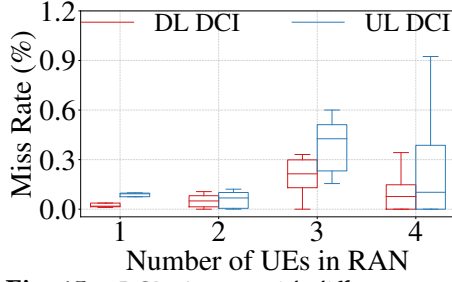


Fig. 15— DCI miss rate with different number of UEs.

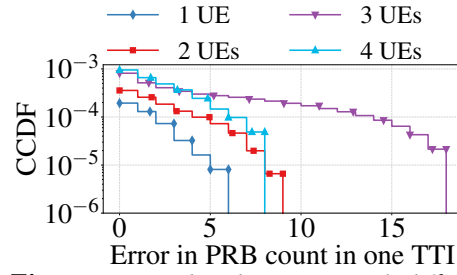


Fig. 16— PRB decoding errors with different number of UEs.

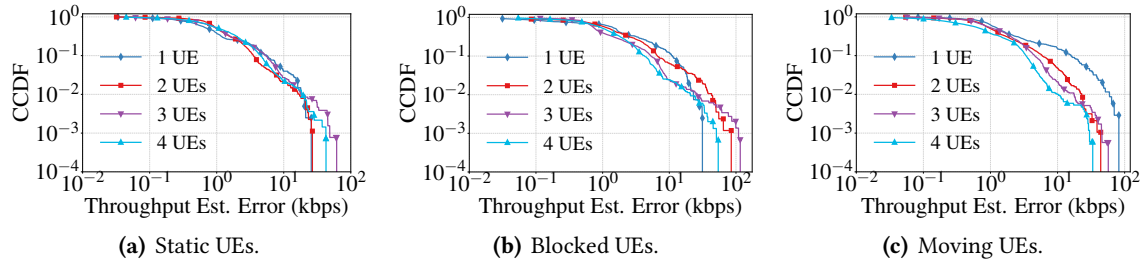


Fig. 17— Accuracy of NG-Scope5G telemetry throughput estimation (ground truth: tcpdump at the UE.)

5.3.2 Decoding accuracy. We evaluate NG-Scope5G telemetry accuracy both via DCI miss rate and PRB decoding accuracy. For this experiment, we use the [srsRAN/Open5GS] fully open-source network. This enables us to collect detailed physical layer *ground truth* for all UEs from srsRAN’s log, in terms of TTI index, DCI content and downlink grants (frequency and time resource allocation, and TBS). We match the number of DCIs captured by NG-Scope5G and srsRAN’s log using the timestamp and the TTI index, through which we calculate a DCI decoding *miss rate*. We use the start and end timestamp and TTI from NG-Scope5G as an *observation period*, and from the observation period, we take all the DCIs from srsRAN’s log as the ground truth. We repeat each evaluation five times; each observation period lasts approximately five minutes.

Firstly, we test the DCI miss rate for each UE, we connect UEs into the srsRAN, and in the mean time use NG-Scope5G to decode the DCIs. Then we match the DCIs decoded by NG-Scope5G and DCIs in srsRAN’s log based on the timestamp and TTI indexes to calculate the miss rate for each UE and put them together to get the distribution. NG-Scope5G achieves a very low DCI miss rate—as Fig. 15 shows, NG-Scope5G detects the vast majority of downlink and uplink DCIs, with miss rates of 0.14% and 0.22%, respectively: two to three 9’s of reliability.

Secondly, we test PRB decoding correctness in the same setting. We compare the downlink and uplink grants decoded by NG-Scope5G and the corresponding grants in the srsRAN log. After we

DCI count:	1	2	3	4
Time (μs):	54 ± 39	71 ± 34	97 ± 33	140 ± 39

Table 2— *Single-thread processing time* per transmission time interval, for different numbers of DCIs in one TTI.

match the DCIs, we compare the decoded number of PRBs with the ground truth within each TTI (0.5 ms with 30 kHz subcarrier spacing) and calculate the number of errors in the NG-Scope5G-decoded PRB count, per TTI. Fig. 16 shows that NG-Scope5G can achieve an average of 0.017 PRB estimation errors per TTI, and most of the time, the PRB estimation error is zero. As we can observe from Fig. 14(b), the number of PRBs allocated for each UE can be up to several hundreds, and so errors of this level will not materially affect the bit rate estimation, as we show next. This demonstrates that NG-Scope5G can decode physical layer PRB information from the base station with high accuracy and granularity.

5.3.3 Throughput estimation accuracy. Here we evaluate the downlink throughput estimation of NG-Scope5G, in our [Mosolabs/Aether] network. In the commercial small cell we do not have access to the physical layer ground truth as we did previously, and so for *ground truth* we instead run tcpdump [50] on the phone to capture network packets, calculate the bit rate and compare the results. We connect different numbers of UE into the small cell, which use the data to watching videos or downloading files, and at the same time we use NG-Scope5G to decode their DCIs. We test the effectiveness of NG-Scope5G under different UE usage scenarios, including static, moving and blocked, to mimic real-life scenarios.

NG-Scope5G achieves a highly accurate bandwidth usage estimation: Fig. 17(a) to 17(c) show the results: NG-Scope5G estimates the UEs' throughput with 75th percentile errors of 2.23, 2.53, and 2.24 Kbit/second in static, blocked, and moving scenarios, respectively. The average downlink bit rate for all UEs is 3.35 Mbit/second in this evaluation, so the 75th percentile bit rate estimation errors are under 0.1%, with errors mainly from missed DCIs.

5.3.4 Processing time. Finally, we demonstrate that NG-Scope5G can operate in real time. We evaluate the signal processing time and DCI translation time of NG-Scope5G in one thread with different number of DCIs in one TTI. A timely processing is vital for telemetry because we need to decode the DCI within the time of one TTI, which ranges from 1 ms for 15 kHz subcarrier spacing, to 0.25 ms for 60 kHz subcarrier spacing in sub-6 GHz bands. In our evaluation, the maximum number of DCIs found in one TTI is four, including both downlink and uplink, and the processing time is shown in Table 2. The data show that NG-Scope5G can process the data efficiently well within the time of one TTI. In this evaluation, we only use one thread of the CPU and so we can easily increase processing capacity by exploiting the parallelism of the task.

6 CONCLUSION

This work has presented the first open-source 5G Standalone RAN passive network telemetry tool, and a telemetry architecture for network applications and end-to-end transport layer protocols that sheds light into the vagaries of the wireless RAN so that they may better adapt their behavior. The NG-Scope5G telemetry tool does not require the cooperation of mobile network operators, chipset manufacturers, or phone manufacturers, nor does it require modifications to the UE. Our mobile cloud gaming implementation and evaluation has demonstrated significant QoE improvements over leading open source game streaming platforms, in a variety of static and mobile settings. Here we use 5G SA telemetry information to schedule downlink traffic (cloud gaming video), but NG-Scope5G can also uplink telemetry information accurately, which can help, *e.g.* web conference and outdoor live streams.

Ethics statement. Cellular telemetry is broadcasted without encryption, so is accessible to anyone with easily-obtainable equipment, and is used here for the sole purpose of communications network design. Telemetry data itself does not identify persons, and the ability to combine the data with another dataset to identify an individual is so attenuated as to be generally impracticable. The relevant IRB has waived the associated master study.

ACKNOWLEDGEMENTS

This material is based upon work supported by the National Science Foundation under Grant Nos. AST-2232457, CNS-2223556 and CNS-2027647. We gratefully acknowledge technical support from the Aether Onramp team to deploy our 5G Standalone cell.

REFERENCES

- [1] 3GPP. Requirements for further advancements for Evolved Universal Terrestrial Radio Access (E-UTRA) (LTE-Advanced). Technical Report (TR) 36.913, 3rd Generation Partnership Project (3GPP), 2008.
- [2] 3GPP. Release 15 Description; Summary of Rel-15 Work Items. Technical Report (TR) 21.915, 3rd Generation Partnership Project (3GPP), 2018.
- [3] 3GPP. Release 16 Description; Summary of Rel-16 Work Items. Technical Report (TR) 21.916, 3rd Generation Partnership Project (3GPP), 2020.
- [4] 3GPP. Release 17 Description; Summary of Rel-17 Work Items. Technical Report (TR) 21.917, 3rd Generation Partnership Project (3GPP), 2022.
- [5] Z. Akhtar, Y. S. Nam, R. Govindan, S. Rao, J. Chen, E. Katz-Bassett, B. Ribeiro, J. Zhan, H. Zhang. Oboe: Auto-Tuning Video ABR Algorithms to Network Conditions. *Proc. of the Conference of the ACM Special Interest Group on Data Communication, SIGCOMM*, 44–58. Association for Computing Machinery, New York, NY, USA, 2018. ISBN 978-1-4503-5567-4. doi:10.1145/3230543.3230558.

- [6] A. Alhilal, T. Braud, B. Han, P. Hui. Nebula: Reliable Low-latency Video Transmission for Mobile Cloud Gaming. *Proceedings of the ACM Web Conference*, 3407–3417. Association for Computing Machinery, New York, NY, USA, 2022. doi:10.1145/3485447.3512276.
- [7] V. Arun, H. Balakrishnan. Copa: Practical Delay-Based Congestion Control for the Internet. *Proc. of the USENIX Symposium on Networked Systems Design and Implementation (NSDI)*. USENIX Association, 2018.
- [8] N. Bui, J. Widmer. OWL: a reliable online watcher for LTE control channel measurements. *Proceedings of the 5th Workshop on All Things Cellular: Operations, Applications and Challenges*, ATC '16, 25–30. Association for Computing Machinery, New York, NY, USA, 2016. ISBN 978-1-4503-4249-0. doi:10.1145/2980055.2980057.
- [9] N. Cardwell, Y. Cheng, C. S. Gunn, S. H. Yeganeh, V. Jacobson. BBR: Congestion-based congestion control. *Queue*, 14(5), 20–53, 2016. Publisher: ACM New York, NY, USA.
- [10] Y. Chen, A. Tahir, F. Yan, R. Mittal. Octopus: In-Network Content Adaptation to Control Congestion on 5G Links. *Eighth ACM/IEEE Symposium on Edge Computing*, 1–16. ACM, Wilmington, DE, 2023. doi:10.1145/3583740.3628438.
- [11] E. Cuervo. Beyond Reality: Head-Mounted Displays for Mobile Systems Researchers. *GetMobile: Mobile Comp. and Comm.*, 21(2), 9–15, 2017. doi:10.1145/3131214.3131218.
- [12] M. Dasari, K. Kahatapitiya, S. R. Das, A. Balasubramanian, D. Samaras. Swift: Adaptive Video Streaming with Layered Neural Codecs. *Proc. of the USENIX Symposium on Networked Systems Design and Implementation (NSDI)*, 2022.
- [13] R. Falkenberg, C. Wietfeld. FALCON: An Accurate Real-Time Monitor for Client-Based Mobile Network Data Analytics. *2019 IEEE Global Communications Conference (GLOBECOM)*, 1–7. Institute of Electrical and Electronics Engineers, Piscataway, NJ, 2019. doi:10.1109/GLOBECOM38437.2019.9014096.
- [14] FCC. 3.5 GHz band overview, 2023.
- [15] S. Fouladi, J. Emmons, E. Orbay, C. Wu, R. S. Wahby, K. Winstein. Salsify: Low-Latency Network Video through Tighter Integration between a Video Codec and a Transport Protocol. *Proc. of the USENIX Symposium on Networked Systems Design and Implementation (NSDI)*. USENIX Association, 2018.
- [16] C. Gutman, D. Waxemberg, A. Neyer, M. Bergeron, A. Hennessy, A. Campbell. Moonlight Mobile Cloud Gaming Client, 2023.
- [17] S. Ha, I. Rhee, L. Xu. CUBIC: A New TCP-friendly High-speed TCP Variant. *SIGOPS Oper. Syst. Rev.*, 42(5), 2008.
- [18] P. Hamadianian, D. Gallatin, M. Alizadeh, K. Chintalapudi. Ekho: Synchronizing Cloud Gaming Media across Multiple Endpoints. *Proc. of the Conference of the ACM Special Interest Group on Data Communication*, SIGCOMM, 533–549. Association for Computing Machinery, New York, NY, USA, 2023. ISBN 9798400702365. doi:10.1145/3603269.3604826.
- [19] T. D. Hoang, C. Park, M. Son, T. Oh, S. Bae, J. Ahn, B. Oh, Y. Kim. LTESniffer: An Open-source LTE Downlink/Uplink Eavesdropper. *Proceedings of the 16th ACM Conference on Security and Privacy in*

- Wireless and Mobile Networks*, 43–48. Association for Computing Machinery, New York, NY, USA, 2023. ISBN 978-1-4503-9859-6. doi:10.1145/3558482.3590196.
- [20] H.-J. Hong, C.-F. Hsu, T.-H. Tsai, C.-Y. Huang, K.-T. Chen, C.-H. Hsu. Enabling Adaptive Cloud Gaming in an Open-Source Cloud Gaming Platform. *IEEE Transactions on Circuits and Systems for Video Technology*, **25**(12), 2078–2091, 2015. doi:10.1109/TCSVT.2015.2450173.
- [21] C.-Y. Huang, C.-H. Hsu, Y.-C. Chang, K.-T. Chen. GamingAnywhere: An Open Cloud Gaming System. *Proceedings of the 4th ACM Multimedia Systems Conference, MMSys '13*, 36–47. Association for Computing Machinery, New York, NY, USA, 2013. ISBN 978-1-4503-1894-5. doi:10.1145/2483977.2483981.
- [22] M. Jarschel, D. Schlosser, S. Scheuring, T. Hoßfeld. Gaming in the clouds: QoE and the users' perspective. *Mathematical and Computer Modelling*, **57**(11), 2883–2894, 2013. ISSN 0895-7177. doi:https://doi.org/10.1016/j.mcm.2011.12.014.
- [23] D. Katabi, M. Handley, C. Rohrs. Congestion control for high bandwidth-delay product networks. *SIGCOMM Comput. Commun. Rev.*, **32**(4), 89–102, 2002. ISSN 0146-4833. doi:10.1145/964725.633035.
- [24] Keysight. Keysight WaveJudge, 2023.
- [25] J. Kim, Y. Jung, H. Yeo, J. Ye, D. Han. Neural-Enhanced Live Streaming: Improving Live Video Ingest via Online Learning. *Proc. of the Conference of the ACM Special Interest Group on Data Communication, SIGCOMM*, 107–125. Association for Computing Machinery, New York, NY, USA, 2020. ISBN 978-1-4503-7955-7. doi:10.1145/3387514.3405856.
- [26] S. S. Krishnan, R. K. Sitaraman. Video stream quality impacts viewer behavior: inferring causality using quasi-experimental designs. *IEEE/ACM Transactions on Networking*, **21**(6), 2001–2014, 2013. ISSN 1063-6692. doi:10.1109/TNET.2013.2281542.
- [27] S. Kumar, E. Hamed, D. Katabi, L. Erran Li. LTE Radio Analytics Made Easy and Accessible. *SIGCOMM Comput. Commun. Rev.*, **44**(4), 211–222, 2014. ISSN 0146-4833. doi:10.1145/2740070.2626320.
- [28] A. A. Laghari, H. He, K. A. Memon, R. A. Laghari, I. A. Halepoto, A. Khan. Quality of experience (QoE) in cloud gaming models: A review. *Multiagent and Grid Systems*, **15**(3), 289–304, 2019. Publisher: IOS Press.
- [29] J. Lee, S. Lee, J. Lee, S. D. Sathyanarayana, H. Lim, J. Lee, X. Zhu, S. Ramakrishnan, D. Grunwald, K. Lee, S. Ha. PERCEIVE: Deep Learning-Based Cellular Uplink Prediction Using Real-Time Scheduling Patterns. *Proceedings of the 18th International Conference on Mobile Systems, Applications, and Services, MobiSys*, 377–390. Association for Computing Machinery, New York, NY, USA, 2020. ISBN 978-1-4503-7954-0. doi:10.1145/3386901.3388911.
- [30] Y. Li, C. Peng, Z. Yuan, J. Li, H. Deng, T. Wang. Mobileinsight: extracting and analyzing cellular network information on smartphones. *Proceedings of the 22nd Annual International Conference on Mobile Computing and Networking, MobiCom*, 202–215. Association for Computing Machinery, New York, NY, USA, 2016. ISBN 978-1-4503-4226-1. doi:10.1145/2973750.2973751.
- [31] LizardByte. Sunshine: a self-hosted game stream host for Moonlight., 2023.
- [32] H. Mao, R. Netravali, M. Alizadeh. Neural Adaptive Video Streaming with Pensieve. *Proc. of the*

- Conference of the ACM Special Interest Group on Data Communication, SIGCOMM*, 197–210. Association for Computing Machinery, New York, NY, USA, 2017. ISBN 978-1-4503-4653-5. doi:10.1145/3098822.3098843.
- [33] F. Metzger, A. Rafetseder, C. Schwartz. A comprehensive end-to-end lag model for online and cloud video gaming. *Proc. 5th ISCA/DEGA Workshop on Perceptual Quality of Systems (PQS 2016)*, 15–19. ISCA, USA, 2016.
 - [34] Mosolab. Mosolab Canopy Small Cell, 2023.
 - [35] Nokia. Fixed Wireless Access Explained. *Newsroom Article*, web, 2023.
 - [36] Nvidia. NVStreams documents., 2023.
 - [37] ONF. ONF Aether Onramp Project, 2023.
 - [38] L. Peterson, O. Sunay. *5G Mobile Networks: A Systems Approach*. Morgan & Claypool, 1st edn., 2020. ISBN 1-68173-890-2.
 - [39] L. Peterson, O. Sunay, B. Davie. *Private 5G: A Systems Approach*. Systems Approach, LLC, 1.1-dev edn., 2022.
 - [40] Qualcomm. It’s time for 5G to Standalone. *OnQ Blog*, web, 2023.
 - [41] RedHat. What is Private 5G? *Technology Topics*, web, 2023.
 - [42] P. Rinderud. Cloud gaming report: Tracing the consumer journey. *Ericsson Blog*, web, 2024.
 - [43] H. Schulzrinne, A. Rao, R. Lanphier. RFC 2396: Real Time Streaming Protocol (RTSP), 1998.
 - [44] H. Schulzrinne, A. Rao, R. Lanphier, W. Westerlund, M. Stiemerling. RFC 7826: Real-Time Streaming Protocol Version 2.0, 2016.
 - [45] ShareTechNote. PDCCH Transmission Process, ShareTechnote, 2023.
 - [46] K. Spiteri, R. Urgaonkar, R. K. Sitaraman. BOLA: Near-Optimal Bitrate Adaptation for Online Videos. *IEEE/ACM Transactions on Networking*, **28**(4), 1698–1711, 2020. ISSN 1063-6692. doi:10.1109/TNET.2020.2996964.
 - [47] Y. Sun, X. Yin, J. Jiang, V. Sekar, F. Lin, N. Wang, T. Liu, B. Sinopoli. CS2P: Improving Video Bitrate Selection and Adaptation with Data-Driven Throughput Prediction. *Proceedings of the 2016 ACM SIGCOMM Conference*, SIGCOMM ’16, 272–285. Association for Computing Machinery, New York, NY, USA, 2016. ISBN 978-1-4503-4193-6. doi:10.1145/2934872.2934898.
 - [48] S. R. System. srsRAN Project: Open Source RAN, 2023.
 - [49] K. Takeda, H. Xu, T. Kim, K. Schober, X. Lin. Understanding the Heart of the 5G Air Interface: An Overview of Physical Downlink Control Channel for 5G New Radio. *IEEE Communications Standards Magazine*, **4**(3), 22–29, 2020. doi:10.1109/MCOMSTD.001.1900048.
 - [50] A. Tcpdump. Official site for the tcpdump binary for Android devices, 2023.
 - [51] S. Wang, S. Yang, H. Li, X. Zhang, C. Zhou, C. Xu, F. Qian, N. Wang, Z. Xu. SalientVR: saliency-driven mobile 360-degree video streaming with gaze information. *Proceedings of the 28th Annual International Conference on Mobile Computing And Networking*, MobiCom ’22, 542–555. Association for Computing Machinery, New York, NY, USA, 2022. ISBN 978-1-4503-9181-8. doi:10.1145/3495243.3517018.
 - [52] A. Webster. Apple opens App Store to game streaming services. *The Verge*, web, 2024.

- [53] K. Winstein, A. Sivaraman, H. Balakrishnan. Stochastic Forecasts Achieve High Throughput and Low Delay over Cellular Networks. *Proc. of the USENIX Symposium on Networked Systems Design and Implementation (NSDI)*, 2013.
- [54] J. Wu, Y. Guan, Q. Mao, Y. Cui, Z. Guo, X. Zhang. ZGaming: Zero-Latency 3D Cloud Gaming by Image Prediction. *Proc. of the Conference of the ACM Special Interest Group on Data Communication, SIGCOMM*, 710–723. Association for Computing Machinery, New York, NY, USA, 2023. ISBN 9798400702365. doi:10.1145/3603269.3604819.
- [55] X. Xie, X. Zhang, S. Zhu. Accelerating Mobile Web Loading Using Cellular Link Information. *Proceedings of the 15th Annual International Conference on Mobile Systems, Applications, and Services, MobiSys*, 427–439. Association for Computing Machinery, New York, NY, USA, 2017. ISBN 978-1-4503-4928-4. doi:10.1145/3081333.3081367.
- [56] Y. Xie, K. Jamieson. NG-Scope: Fine-Grained Telemetry for NextG Cellular Networks. *Proc. ACM Meas. Anal. Comput. Syst.*, **6**(1), 1–26, 2022. doi:10.1145/3508032.
- [57] Y. Xie, F. Yi, K. Jamieson. PBE-CC: Congestion Control via Endpoint-Centric, Physical-Layer Bandwidth Measurements. *Proc. of the Conference of the ACM Special Interest Group on Data Communication, SIGCOMM*, 451–464. Association for Computing Machinery, New York, NY, USA, 2020. ISBN 978-1-4503-7955-7. doi:10.1145/3387514.3405880.
- [58] F. Y. Yan, H. Ayers, C. Zhu, S. Fouladi, J. Hong, K. Zhang, P. Levis, K. Winstein. Learning in Situ: A Randomized Experiment in Video Streaming. *Proc. of the USENIX Symposium on Networked Systems Design and Implementation (NSDI)*, 495–512. USENIX Association, USA, 2020. ISBN 978-1-939133-13-7.
- [59] X. Yin, A. Jindal, V. Sekar, B. Sinopoli. A Control-Theoretic Approach for Dynamic Adaptive Video Streaming over HTTP. *SIGCOMM Comput. Commun. Rev.*, **45**(4), 325–338, 2015. ISSN 0146-4833. doi:10.1145/2829988.2787486.

A TRANSPORT BLOCK SIZE CALCULATION

The following development restates the 3GPP standard TBS calculation [4] for convenience here.

Firstly, we calculate the intermediate variable N_{RE} :

$$N'_{RE} = N_{sc}^{RB} \times N_{symb}^{sh} - N_{DMRS}^{PRB} - N_{oh}^{PRB}, \quad (5)$$

$$N_{RE} = \min(156, N'_{RE}) * n_{PRB}. \quad (6)$$

N_{sc}^{RB} is the number of subcarriers per resource block and it's 12. N_{symb}^{sh} is the number of time domain OFDM symbols allocated through DCI, which can be found in t_{alloc} in the DCI grant in Appendix C.3. N_{DMRS}^{PRB} is the number of resource elements for DMRS per PRB and N_{oh}^{PRB} is the overhead of PDSCH, which are both defined in RRC messages. n_{PRB} is the frequency domain resource block allocated by DCI, which can be found in f_{alloc} in the DCI grant in Appendix C.3. N_{RE} represents the effective resource elements (1 OFDM symbol \times 1 subcarrier) allocated for the UE in the DCI.

The second step is to calculate N_{info} :

$$N_{info} = N_{RE} \times R \times Q_m \times v. \quad (7)$$

R is the code rate and Q_m is the modulation order, which are delivered through the DCI's MSC value and the UE checks the predefined tables with it [4]. And v is number of layers, transferred in the MSG 4's element "*pdsch – ServingCellConfig*": "*maxMIMO – Layers*".

The final step is to calculate the TBS, which contains some value determination:

- If $N_{info} \leq 3824$, we have $N'_{info} = 2^n \times \text{round}(\frac{N_{info}-24}{2^n})$, where $n = \lfloor \log_2(N_{info} - 24) \rfloor - 5$.
Then, if $R \leq 1/4$, we have $TBS = 8C \lceil \frac{N'_{info}+24}{8C} \rceil - 24$, where $C = \lceil \frac{N'_{info}+24}{3814} \rceil$. If $R > 1/4$, we have $TBS = 8 \lceil \frac{N'_{info}+24}{8} \rceil - 24$ if $N'_{info} < 8424$, and $TBS = 8C \lceil \frac{N'_{info}+24}{8C} \rceil - 24$ if $N'_{info} \geq 8424$, where $C = \lceil \frac{N'_{info}+24}{8424} \rceil$.
- If $N_{info} > 3824$, we have $N'_{info} = \max(24, 2^n \lfloor \frac{N_{info}}{2^n} \rfloor)$, where $n = \max(3, \lfloor \log_2(N_{info}) \rfloor - 6)$. Then we check table 5.1.3.2-2 in [4] to determine the TBS.

B RTSP INTRODUCTION

RTSP is an application layer protocol that the server and client use to set up real-time streams. The detailed RTSP handshake message flow is shown in Fig. 18, the client sends request messages and the server replies the corresponding information. The client first sends "OPTION" request to ask other RTSP messages that the RTSP server supports, in sunshine, the other supported RTSP messages are "DESCRIBE", "SETUP", "ANNOUNCE", and "PLAY", as in Fig. 18. Then, the client sends "DESCRIBE" message to ask the streams that the server provides, where in the gaming platform are downlink video and audio streams and uplink user input stream. With these information, the client asks about the ports of these streams it wants to connects through multiple "SETUP" messages. When the client is ready to connect to these streams, it tells the gaming server through "ANNOUNCE" message. Then the client sends the "PLAY" message to actually start the gaming service.

After the gaming client tells the telemetry server the IP and port of the gaming server, the telemetry server can use the similar messages exchange ("OPTION" to "PLAY") to connect to the server's feedback stream. Since the RTSP server is implemented in a event-driven way, the telemetry server's RTSP handshake can happen anytime even in the middle of client's RTSP handshake, not strictly ordered as in Fig. 18.

C SAMPLE OF RRC MESSAGE

We list some key components in SIB 1 and MSG 4 here.

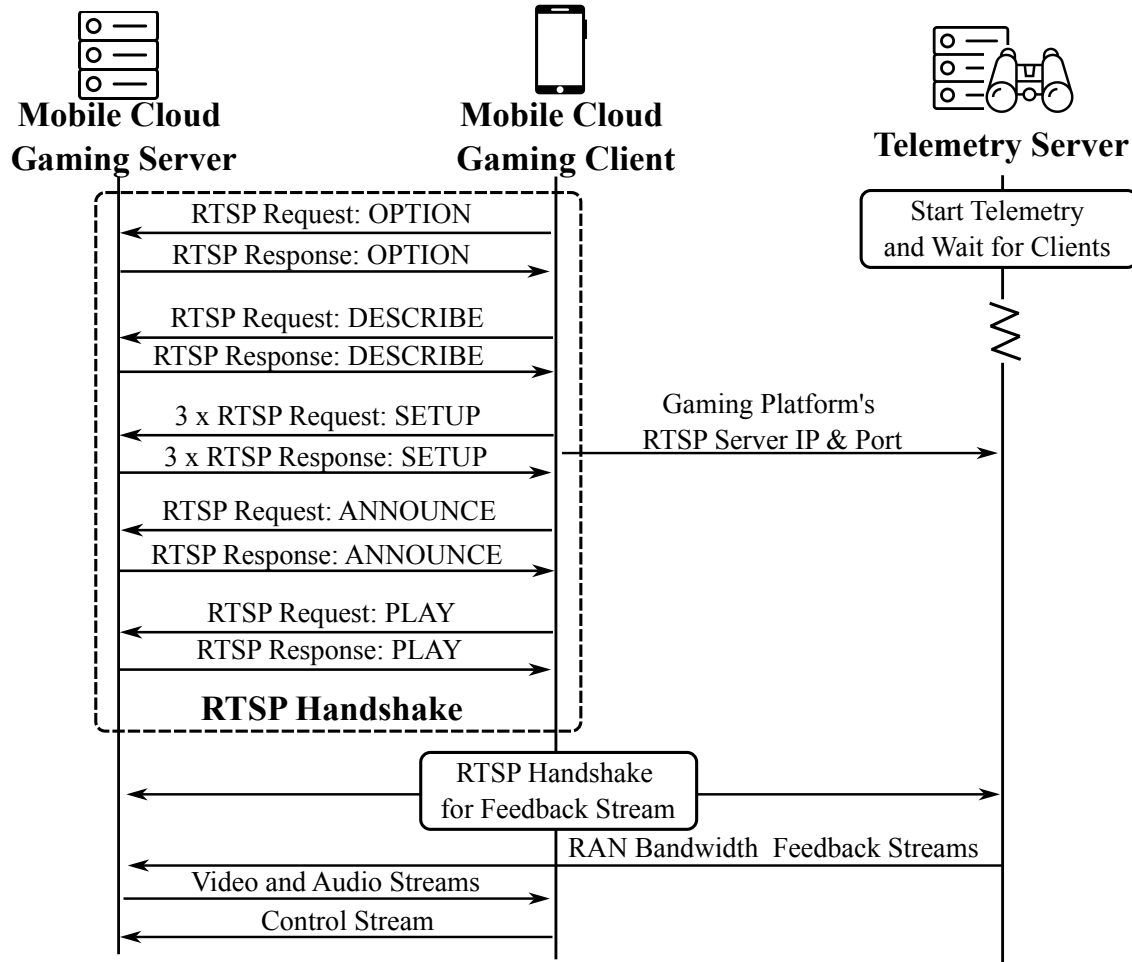


Fig. 18— RTSP initiated data flow between mobile cloud gaming server, client and telemetry server.

C.1 SIB 1 Sample

The key components for telemetry in SIB 1 that we decoded from the Sercomm small cell are shown as below:

```
"SIB1": {
  ...
  "servingCellConfigCommon": {
    "downlinkConfigCommon": {
      "frequencyInfoDL": {
        "frequencyBandList": [
          {
```



```

        "freqBandIndicatorNR": 48
    }
],
"offsetToPointA": 24,
"scs-SpecificCarrierList": [
    {
        "offsetToCarrier": 0,
        "subcarrierSpacing": "kHz30",
        "carrierBandwidth": 51
    }
]
},
"initialDownlinkBWP": {
    "genericParameters": {
        "locationAndBandwidth": 13750,
        "subcarrierSpacing": "kHz30"
    },
    "pdcch-ConfigCommon": {
        {
            "controlResourceSetZero": 10,
            "searchSpaceZero": 0,
            "commonSearchSpaceList": [
                {
                    "searchSpaceId": 1,
                    "controlResourceSetId": 0,
                    "monitoringSlotPeriodicityAndOffset": {
                    },
                    "monitoringSymbolsWithinSlot":
                        "10000000000000",
                    "nrofCandidates": {
                        "aggregationLevel1": "n0",
                        "aggregationLevel2": "n0",
                        "aggregationLevel4": "n2",
                        "aggregationLevel8": "n0",
                        "aggregationLevel16": "n0"
                    },
                    "searchSpaceType": {
                        "common": {
                            "dci-Format0-0-AndFormat1-0": {
                            }
                        }
                    }
                }
            ]
        }
    }
}

```

```

        }
    ],
    "searchSpaceSIB1": 0,
    "searchSpaceOtherSystemInformation": 1,
    "pagingSearchSpace": 1,
    "ra-SearchSpace": 1
}
},
"pdsch-ConfigCommon": {
    {
        "pdsch-TimeDomainAllocationList": [
            {
                "k0": 0,
                "mappingType": "typeA",
                "startSymbolAndLength": 53
            },
            {
                "k0": 0,
                "mappingType": "typeA",
                "startSymbolAndLength": 67
            }
        ]
    }
}
},
"bcch-Config": {
    "modificationPeriodCoeff": "n2"
},
"pcch-Config": {
    "defaultPagingCycle": "rf64",
    "nAndPagingFrameOffset": {
    },
    "ns": "one",
    "firstPDCCH-MonitoringOccasionOfPO": {
        "sCS30KHzZoneT-SCS15KHzHalfT": [
            1
        ]
    }
}
},
...
}.

```

C.2 MSG 4 Sample

The key components for telemetry in MSG 4 that we decoded from the Sercomm small cell are shown as follow:

```
"RRCSetup": {
  ...
  "masterCellGroup": {
    ...
    "physicalCellGroupConfig": {
      "p-NR-FR1": 26,
      "pdsch-HARQ-ACK-Codebook": "dynamic"
    },
    "spCellConfig": {
      "rlmInSyncOutOfSyncThreshold": "n1",
      "spCellConfigDedicated": {
        "initialDownlinkBWP": {
          "pdcch-Config": {
            {
              "controlResourceSetToAddModList": [
                {
                  "controlResourceSetId": 1,
                  "frequencyDomainResources":
                    "11111111000000000000...",
                  "duration": 2,
                  "cce-REG-MappingType": {
                    },
                  "precoderGranularity": "allContiguousRBs",
                  "pdcch-DMRS-ScramblingID": 5
                }
              ],
              "searchSpacesToAddModList": [
                {
                  "searchSpaceId": 2,
                  "controlResourceSetId": 1,
                  "monitoringSlotPeriodicityAndOffset": {
                    },
                  "monitoringSymbolsWithinSlot":
                    "10000000000000",
                  "nrofCandidates": {
                    "aggregationLevel1": "n4",
                    "aggregationLevel2": "n4",
                    "aggregationLevel4": "n2",
```

```

        "aggregationLevel18": "n1",
        "aggregationLevel16": "n0"
    },
    "searchSpaceType": {
        "ue-Specific": {
            "dci-Formats": "formats0-1-And-1-1"
        }
    }
}
]
}
},
"pdsch-Config": {
    {
        "dataScramblingIdentityPDSCH": 5,
        "dmrs-DownlinkForPDSCH-MappingTypeA": {
            {
                "dmrs-AdditionalPosition": "pos1"
            }
        },
        "resourceAllocation":
            "resourceAllocationType1",
        "pdsch-TimeDomainAllocationList": {
            [
                {
                    "k0": 0,
                    "mappingType": "typeA",
                    "startSymbolAndLength": 53
                },
                {
                    "k0": 0,
                    "mappingType": "typeA",
                    "startSymbolAndLength": 67
                }
            ]
        },
        "rbg-Size": "config1",
        "maxNrofCodeWordsScheduledByDCI": "n1",
        "prb-BundlingType": {
            "staticBundling": {
                "bundleSize": "wideband"
            }
        }
    }
}

```

```

    }
  }
},
"firstActiveDownlinkBWP-Id": 0,
"defaultDownlinkBWP-Id": 0,
"uplinkConfig": {
  "initialUplinkBWP": {
    "pucch-Config": {
      {
        ...
      }
    },
    "pusch-Config": {
      {
        "dataScramblingIdentityPUSCH": 5,
        "dmrs-UplinkForPUSCH-MappingTypeA": {
          {
            "dmrs-AdditionalPosition": "pos1",
            "transformPrecodingDisabled": {
              "scramblingID0": 5
            }
          }
        }
      }
    },
    "pusch-PowerControl": {
      "tpc-Accumulation": "disabled",
      "msg3-Alpha": "alpha1",
      "p0-AlphaSets": [
        {
          "p0-PUSCH-AlphaSetId": 0,
          "p0": 0,
          "alpha": "alpha1"
        }
      ],
      "deltaMCS": "enabled"
    },
    "resourceAllocation":
      "resourceAllocationType1",
    "pusch-TimeDomainAllocationList": {
      [
        {
          "k2": 4,

```

```

        "mappingType": "typeA",
        "startSymbolAndLength": 55
    },
    ...
]
},
"transformPrecoder": "disabled",
...
}
}
},
"firstActiveUplinkBWP-Id": 0
},
"pdsch-ServingCellConfig": {
    {
        "nrofHARQ-ProcessesForPDSCH": "n16",
        "maxMIMO-Layers": 2
    }
},
"tag-Id": 0
}
}
}
}
}

```

C.3 DCI and Grant

A downlink DCI looks like:

DCI:

```

c-rnti=0x4296,
dci=1_1,
ss=ue,
L=0,
cce=7,
f_alloc=0x33,
t_alloc=0x0,
mcs=27,
ndi=0,
rv=0,
harq_id=11,
dai=2,
tpc=1,

```

```

harq_feedback=2,
ports=7,
srs_request=0,
dmrs_id=0

```

And its translated grant for PDSCH is like:

DMRS:

```

type=1
add_pos=2
len=single
typeA_pos=2
rvd_pattern:
    begin=0
    end=275
    stride=1
    sc=111111111111
    symb=00100001000100

```

Grant:

```

rnti=0x4296
rnti_type=C-RNTI
k=0
mapping=A
t_alloc=2:12
f_alloc=0:2
nof_dmrs_cdm_grps=2
beta_dmrs=1.412538
nof_layers=2
n_scid=0
tb_scaling_field=0
CW0:
    mod=256QAM
    nof_layers=2
    mcs=27
    tbs=3240
    R=0.926
    rv=0
    ndi=0
    nof_re=432
    nof_bits=3456

```

SCH:

```

mcs_table=256qam
xoverhead=0

```